Capturing patterns and symmetries in chaotic granular flow

Steven W. Meier,[1] Stephen E. Cisar,[1] Richard M. Lueptow,[2,*] and Julio M. Ottino[1,2]
[1]*Department of Chemical and Biological Engineering, Northwestern University, Evanston, Illinois 60208, USA*
[2]*Department of Mechanical Engineering, Northwestern University, Evanston, Illinois 60208, USA*
(Received 26 April 2006; published 27 September 2006)

Segregation patterns formed by time-periodic flow of polydisperse granular material (varying in particle size) in quasi-two-dimensional (quasi-2D) tumblers capture the symmetries of Poincaré sections, stroboscopic maps of the underlying flow, derived from a continuum model which contains no information about particle properties. We study this phenomenon experimentally by varying the concentration of small particles in a bidisperse mixture in quasi-2D tumblers with square and pentagonal cross sections. By coupling experiments with an analysis of periodic points, we explain the connection between the segregation patterns and the dynamics of the underlying flow. Analysis of the eigenvectors and unstable manifolds of hyperbolic points shows that lobes of segregated small particles stretch from hyperbolic points toward corners of the tumbler, demonstrating the connection between regions of chaotic flow and the shape of the segregation patterns. Furthermore, unstable manifolds map the shape of lobes of segregated particles. The techniques developed here can also be applied to nonpolygonal tumblers such as elliptical tumblers, as well as to circular tumblers with time-periodic forcing.

DOI: 10.1103/PhysRevE.74.031310 PACS number(s): 45.70.Mg, 45.70.Qj, 47.52.+j, 47.57.Gc

I. INTRODUCTION

A distinguishing feature of flowing granular matter is the tendency to segregate; mixtures of particles with varying size (*S* systems) or varying density (*D* systems) subject to flow often segregate leading to what on first viewing appear to be baffling results [1–4]. In *D* systems, the heavier particles are driven by gravity lower in the flowing layer, forcing the lighter particles toward the top due to buoyancy forces [5–7]. In *S* systems, smaller particles will percolate through the spaces between the larger particles and segregate toward the bottom of the layer pushing the large particles toward the top [8–11].

An example of size segregation in a half-full quasi-two-dimensional (quasi-2D) square tumbler is shown on the left side of Fig. 1. Initially the tumbler is partially filled with a mixture of particles of two different sizes. The tumbler is rotated at a rate where the flow is in the rolling regime (also referred to as the continuous-flow regime) [2–4,12–14]. As the tumbler rotates, the particles near the surface flow in a thin layer. Particles enter this layer on the upstream end from a near-static fixed bed in solid body rotation with the tumbler. Particles exit the flowing layer on the downstream end of the flowing layer. The net result of the percolation of smaller particles in the thin surface flowing layer coupled with the time-periodic flow due to tumbler geometry is the formation of a core having two lobes rich in small black particles near the center of the tumbler with a region rich in large clear particles near the periphery, as shown in the left portion of Fig. 1.

The computationally derived Poincaré section in the right portion of Fig. 1 is a stroboscopic mapping of a few points initially placed in a square tumbler and advected according to a kinematic continuum model of the flow without consideration of segregation [15]. The Poincaré section captures the time-periodic behavior of the flow. Such Poincaré sections can also be generated using a discrete mapping of granular flows in rotating tumblers rather than based on a continuum model [16]. Some points in the Poincaré section are confined to islands along the diagonals, while others are advected over much of the tumbler [1]. What is surprising is that the structure of the segregation pattern on the left shows remarkable similarity with that of the Poincaré section on the right, in spite of the very different means by which the two figures are generated. The computational model used to generate the Poincaré section contains no information on particle properties or segregation. The medium is taken to be monodisperse. Despite the difference between the bidisperse experiment and the monodisperse model, the smaller particles in the experiment form lobes that overlap with the location of the islands in the Poincaré section. In this paper we examine to what extent and why experimental segregation patterns and computationally derived Poincaré sections appear to capture the same patterns and symmetries in time-periodic granular flow.

Insight into the relationship between Poincaré sections and flow in physical bidisperse systems can be obtained from techniques commonly applied to chaotic mixing in fluids. Dye experiments in mixing of fluids, primarily for time-periodic flows, have been instrumental over the last two decades in yielding insights into the working of chaotic flows. Strategically placed colored blobs, after a few periods of the flow, produce persistent large scale structures—templates of the manifold structure or the chaotic nature of the flow [17]. Typically, colored blob experiments reveal regions of chaotic mixing. In the case of the half-full square in Fig. 1, the chaotic region of the flow is everything outside of the islands. Blob experiments have been attempted in granular flows [18]. However, forming a blob in granular matter is difficult. Moreover, very quickly the granular "blob" becomes broken and the connectivity of the "dyed" structure is lost, as opposed to the companion fluid case where the

*Electronic address: r-lueptow@northwestern.edu

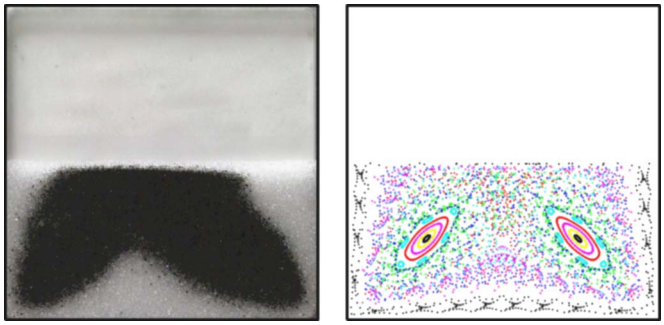

FIG. 1. (Color online) Left: segregation experiment in half-full square tumbler with 40% small (0.3 mm) black particles and 60% large (1.2 mm) clear particles by weight. Steady state pattern after 10 clockwise revolutions of the tumbler at 1.44 RPM. Right: Poincaré section of half-full square.

stretching and folding of the fluid continuum is readily visible. Segregation experiments in granular matter, on the other hand, tend to make visible regions in which islands occur, as shown in Fig. 1. Thus, granular and fluid experiments highlight different aspects of the underlying chaotic flows—and in some sense they may be imagined as complementary, like the positive and negative images of a photograph. Where dye experiments in fluids identify chaotic regions, segregation experiments in granular matter identify islands.

Although it is apparent that the lobes in segregation experiments have some connection with the islands in Poincaré sections, the nature of the relationship is unclear. In particular, can the patterns of segregated small particles always be predicted by the islands? After all, Poincaré sections are computed from a simple kinematic continuum model that does not contain any information about particle segregation. We approach these issues through both experiment and numerical analysis by studying quasi-2D square, pentagonal, elliptical, and circular tumblers of varying fill fractions. The extent to which segregating granular materials reveal the underlying flow as displayed by Poincaré sections is explored by varying the concentration of small particles in segregation experiments. Numerical techniques borrowed from fluid mixing studies further expand our understanding of the relationship between segregation patterns and Poincaré sections.

II. TIME-PERIODIC FLOW

A Poincaré section such as a stroboscopic map provides information about the time-periodic nature of the underlying flow in the tumbler. Points are initially placed throughout the tumbler. The points are then advected according to a continuum model, and their locations are plotted after each period of flow as described below. Some points explore much of the domain of the tumbler, while other points are trapped in islands, such as those in the Poincaré section in Fig. 1 along the diagonals of the tumbler. These different regions of the flow can be characterized in terms of periodic points. A periodic point is a point that returns to its initial position after some number of iterations of a time-periodic flow or mapping. Consider a point $\mathbf{x}(x,y)$ with an initial location $\mathbf{x}_0$. A mapping function $\mathbf{F}$ describes the advection of $\mathbf{x}$ through one period of flow. The location of $\mathbf{x}$ after n iterations of a mapping is

$$\mathbf{x}_n = \mathbf{F}^n \mathbf{x}_0. \tag{1}$$

If $\mathbf{x}_0 = \mathbf{P}$, $\mathbf{x}_n = \mathbf{P}$, and $\mathbf{x}_m \neq \mathbf{P}$ where $m < n$, then $\mathbf{P}$ is a periodic point of order n. In general, a periodic point is a period-n point if that point returns to its initial position after n iterations.

The nature of the periodic point provides information about the character of the flow in the surrounding region [19]. There are three different types of periodic points: elliptic, hyperbolic, and parabolic. The behavior of the flow near elliptic points is the subject of the Kolmogorov-Arnold-Moser (KAM) theorem [20–22]. Particles initially located near a period-n elliptic point return to the vicinity of that elliptic point after n periods of flow. There is also a rotation or twist of the material near the elliptic point [23]. In the generation of a Poincaré section, points initially placed near an elliptic point and plotted each time period tend to form closed rings, such as the ellipse-like rings that make up the islands along the diagonals in the Poincaré section in Fig. 1. The closed rings are examples of KAM structures. Points cannot cross these structures, so that material outside the KAM structure stays outside and material inside the KAM structure stays inside. Since these structures are barriers to mixing of material they are often referred to as islands [19,24,25]. An island is of period n if it is characterized by a period-n elliptic point. In general, larger islands have lower order elliptic points [26]. The islands in Fig. 1 are period-2 because the elliptic points that characterize them return to their initial positions every two periods of one-quarter revolution.

In the case of a granular tumbler, the mapping $\mathbf{F}$ comes from integration of the velocity field in the tumbler [1,15,27]. We apply a simple 2D kinematic continuum model for the velocity field to study the underlying flow. All dynamics of the flow occur in a thin rapidly flowing surface layer that is typically a maximum of 5–10 particles thick [28]. Below the surface layer is an essentially static or fixed bed of particles in solid body rotation with the tumbler. Setting the origin of the coordinate system at the midpoint of the free surface with x in the streamwise direction and y normal to the surface directed upward, the flow in this surface layer is given by

$$v_x(x,y) = 2u\left(1 + \frac{y}{\delta(x)}\right), \tag{2}$$

$$v_y(x,y) = -\omega x\left(\frac{y}{\delta(x)}\right)^2, \tag{3}$$

where the depth averaged velocity in the flowing layer $u = \omega L^2/2\delta_0$, ω is the rotation rate of the tumbler, and L is the distance from the origin to the tumbler wall, where $2L$ is referred to as the flowing layer length [1,15]. The flowing layer thickness $\delta(x)$ is modeled as parabolic with a maximum of δ_0 at $x=0$ [1,15].

$$\delta = \delta_0 \left[1 - \left(\frac{x}{L} \right)^2 \right]. \tag{4}$$

Previous experiments in laboratory scale tumblers have shown that δ_0 is proportional to L [18]. In the tumbler geometries discussed here, L is time periodic. For example, in a half-full square tumbler, L is a maximum when the flowing layer is along the diagonal and a minimum when the flowing layer is parallel to a wall. This occurs four times for each revolution of the tumbler (so a period is one-quarter revolution). In general, for a N-sided polygonal tumbler, a period is $\frac{1}{N}$ revolutions. (For elliptical and circular tumblers, the periodicity of the flow is defined differently and will be discussed later.) The mapping $\mathbf{F}$ involves the tracking of the motion of a particle via the integration of the velocity field through the flowing layer using Eqs. (2) and (3), as well as through the solid body rotation in the fixed bed of the tumbler.

Periodic points tend to be found in symmetric pairs. The symmetries can be found from geometric insight and some basic knowledge of the underlying flow [23]. Consider the half-full square tumbler in Fig. 1. Based on the Poincaré section, elliptic points are expected to lie along diagonals between the bottom corners and the center of rotation. To find the elliptic points, a series of points separated by a small distance are placed along the diagonal and then advected according to the model for the number of periods that correspond to the order of the periodic point in question. The point that moves the least from its initial position is noted and a new line of points is placed along the diagonal near this point but with a much smaller separation distance. The process is repeated until a point is identified along the line that moves less than some tolerance, typically on the order of the computational precision of the calculations. The location $(\bar{x},\bar{y})$ of this point is the periodic point. A similar method is used to find the hyperbolic points, except that the points are placed along a line between the center of the tumbler and the midpoint of the bottom wall, based on the Poincaré section.

The type of periodic point (elliptic, hyperbolic, and parabolic) can be identified in the following way. By computing the Jacobian, $\mathbf{J}$, of the linearization of mapping $\mathbf{F}$ near a periodic point, its type can be identified by the eigenvalues λ_1 and λ_2 [29]. Note that when $\det(\mathbf{J})=1$, $\lambda_1\lambda_2=1$. If $\lambda_{1,2}=A\pm iB$ where $B\neq 0$, then the point is elliptic. The islands in the Poincaré section in Fig. 1 are characterized by period-2 elliptic points. If $\lambda_{1,2}$ are both real ($B=0$) and $A\neq\pm 1$, then the point is hyperbolic. Hyperbolic points are related to stretching and compression in the flow. Regions around hyperbolic points are typically chaotic. The eigenvalue with modulus greater than one has an eigenvector that corresponds to the direction of stretching. The eigenvalue with modulus less than one has an eigenvector that corresponds to the direction of compression. There are two period-2 hyperbolic points that lie within the regions of chaotic flow in the half-full square in Fig. 1 (one near the center of the fixed bed of granular material and one in the flowing layer). If $\lambda_{1,2}=\pm 1$, the point is parabolic. Parabolic points characterize steady shear flow and are not of interest in this paper (since the flows here are time periodic, not steady).

The terms in the Jacobian matrix are derived from four points placed around the periodic point of interest $(\bar{x},\bar{y})$: $(\bar{x}+\epsilon,\bar{y}),(\bar{x}-\epsilon,\bar{y}),(\bar{x},\bar{y}+\epsilon),(\bar{x},\bar{y}-\epsilon)$. The spacing ϵ is typically very small (in this case, $\epsilon/L_{\min}=0.001$, where $L_{\min}$ is the minimum value of L). The Jacobian matrix of the linearized mapping is defined as

$$\mathbf{J} = \begin{bmatrix} J_{xx} & J_{xy} \\ J_{yx} & J_{yy} \end{bmatrix}, \tag{5}$$

where

$$J_{xx} = \frac{x_n(\bar{x}+\epsilon,\bar{y}) - x_n(\bar{x}-\epsilon,\bar{y})}{2\epsilon}, \tag{6a}$$

$$J_{xy} = \frac{x_n(\bar{x},\bar{y}+\epsilon) - x_n(\bar{x},\bar{y}-\epsilon)}{2\epsilon}, \tag{6b}$$

$$J_{yx} = \frac{y_n(\bar{x}+\epsilon,\bar{y}) - y_n(\bar{x}-\epsilon,\bar{y})}{2\epsilon}, \tag{6c}$$

$$J_{yy} = \frac{y_n(\bar{x},\bar{y}+\epsilon) - y_n(\bar{x},\bar{y}-\epsilon)}{2\epsilon}, \tag{6d}$$

where the subscript n is the number of iterations of the periodic mapping as defined previously [29]. The accuracy check comes from verifying that $\det(\mathbf{J})=1$ within some tolerance based on the precision of the computations. These points are then advected for the number of periods that correspond to the period of point $(\bar{x},\bar{y})$ (i.e., for a period-n point, the points are advected for n periods). Then the Jacobian can be calculated from the equations above and the eigenvalues calculated from $\det(\mathbf{J}-\lambda\mathbf{I})=0$, where $\mathbf{I}$ is the identity matrix. With the eigenvalues and the Jacobian in hand, the corresponding eigenvectors can be found.

III. CAPTURING PATTERNS

The extent to which segregation experiments capture the symmetries of the Poincaré section is explored using square and pentagonal tumblers. For the experiments, the square tumbler is 157 mm on a side and the pentagonal tumbler is 141 mm on a side. Since the tumblers are only 6 mm thick in the axial direction, they are considered to be quasi-2D. The dynamics that create the patterns we study here are essentially 2D since there is negligible axial flow of particles. In the bidisperse experiments, the large particles are 1.21 ± 0.04 mm clear glass beads while the small particles are 0.29 ± 0.01 mm painted black glass beads. The rotation rate of the tumbler is set at 1.44 revolutions per minute, clockwise, fast enough so the flow is in the rolling (continuous-flow) regime. Images are taken with a four megapixel Canon digital camera. Numerical Poincaré sections corresponding to the experimental conditions are generated by placing 13 evenly spaced points in the lower half of the tumbler along the diagonal extending from the center to the lower left corner of the tumbler. The points are then advected for 500 periods of flow and their locations are plotted at the end of

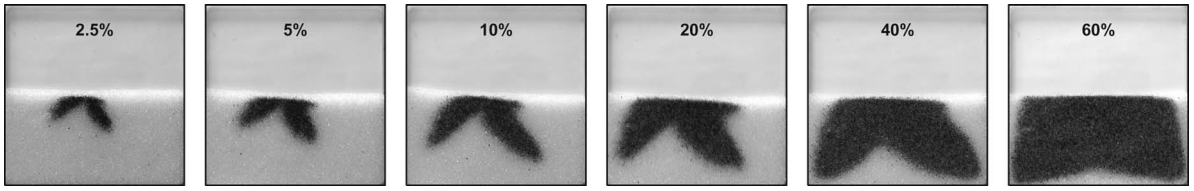

FIG. 2. Series of segregation experiments in half-full square tumbler with varying concentrations of small black particles by weight percent.

each period. An underlying assumption in the connection between the segregation patterns and the symmetries of the underlying dynamics displayed in the Poincaré section is that the velocity field in the flowing layer [Eqs. (2)–(4)] is independent of the particle type. For particular particle types, size, and density combinations, particle-to-tumbler size ratios, fill fractions, and rotation rates, radial streaks of segregated particles can sometimes be observed rather than patterns resembling the symmetries of the Poincaré section [1,6,7,30,31]. However, for the particle types, rotation rate, and fill fractions considered in this paper, streak patterns were not observed.

First we consider segregation in a half-full square tumbler by varying the concentration of small particles. Figure 2 shows experimental results for trials with concentrations of small black particles ranging from 2.5 to 60 % by weight (corresponding to measured volume fractions of 1.3 to 58.8 %). In all cases, small particles segregate to form two lobes extending toward the corners of the tumbler. The segregation is imperfect. Clear beads are interspersed among the small black beads. For lower concentrations the lobes stretch along the diagonals of the square tumbler, but are shifted slightly clockwise. The lobe on the right side appears to be larger in these images because a portion of the left lobe has already entered the flowing layer. In the 40% by weight case, the lobes do not stretch much further than the 20% case but are much thicker. At 60% by weight, the lobes are very thick and appear to be symmetric about the vertical midline. This observation yields insights into the tendency of the lobes of segregated particles to move toward the location of islands, as will be discussed later. The presence of lobes even for low concentrations (less than 10% by weight) suggests that the segregation pattern is shaped by the underlying dynamics of the flow in the chaotic regions rather than simply marking the location of the islands.

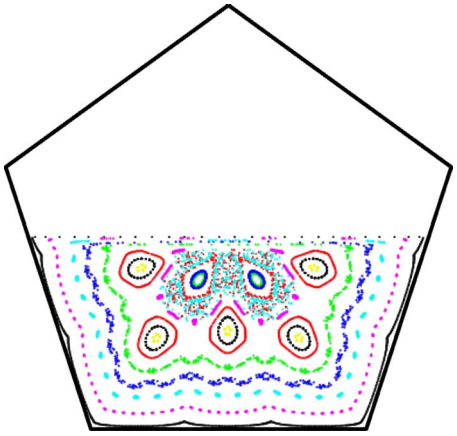

FIG. 3. (Color online) Poincaré section of a half-full pentagonal tumbler.

Previous experiments have shown a wide range of patterns for tumblers of different geometries and different fill fractions [1,27]. Examining a variety of different systems provides insight into the relationship between the Poincaré section and segregation patterns. Using the half-full square as reference, we can change the dynamics of the flow in two ways: fill fractions can be altered from half-full, or the number of sides of the tumbler can be changed (in this case a regular pentagonal tumbler).

First consider the higher-order geometry of a half-full pentagonal tumbler, the Poincaré section for which is shown in Fig. 3. In this case, one period of flow is one-fifth revolution. Unlike the half-full square tumbler, a half-full pentagonal tumbler has two maxima in flowing layer length during each period (and hence streamwise velocity, v_x): one where the flowing layer intersects a corner on the right side of the tumbler and one where it intersects a corner on the left side. Instead of the period-2 islands in the half-full square, the Poincaré section for the pentagon has period-2 islands near the center, surrounded by period-5 islands. Unlike the half-full square tumbler, the Poincaré section shows a smaller region of chaotic flow.

Figure 4 shows experiments in a half-full pentagonal tumbler using mixtures that are 10, 30, and 50 % by weight small particles. For a mixture of 10% by weight small particles, the small particles form a pattern with two lobes ex-

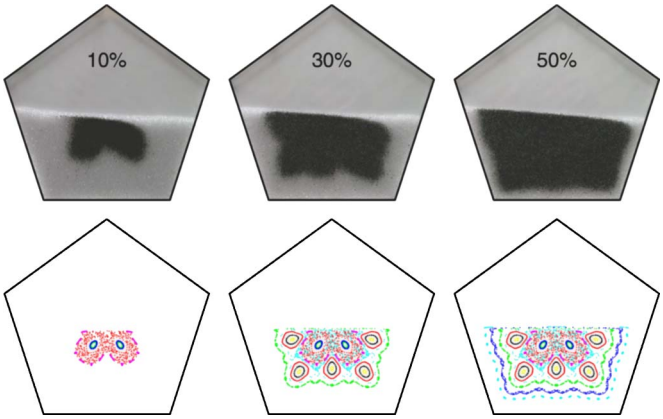

FIG. 4. (Color online) Comparison of segregation experiments to Poincaré sections for half-full pentagonal tumbler. Top: segregation experiments varying the concentration by weight of small particles. Bottom: Poincaré sections with the initial locations of points chosen so the patterns correspond to areas occupied by small particles.

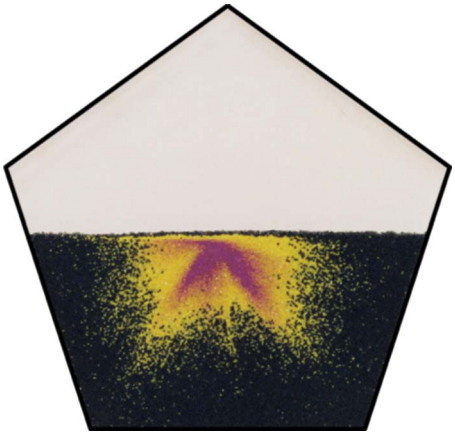

FIG. 5. (Color online) Polydisperse segregation experiment in a half-full pentagonal tumbler.

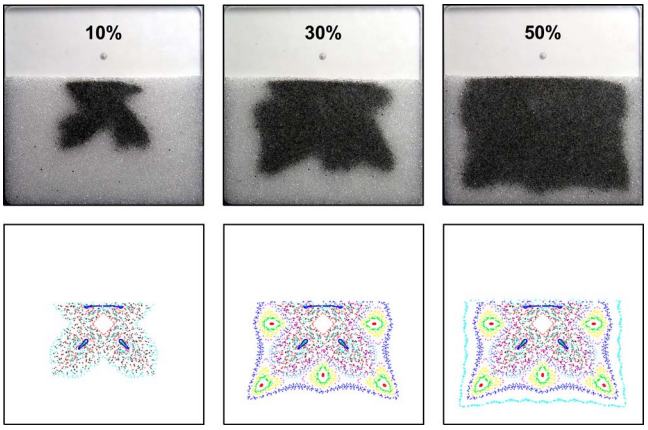

FIG. 6. (Color online) Comparison of segregation experiments to Poincaré sections for 63%-full square tumbler. Top: segregation experiments varying small particle concentration in weight percent. Bottom: Poincaré sections with the initial locations of points chosen so the patterns correspond to areas occupied by small particles.

tending from the center toward each of the bottom corners. The corresponding Poincaré section obtained using only a few initial points clustered near the center of rotation (leftmost Poincaré section in the lower row of Fig. 4) displays period-2 islands in the underlying flow that match the lobes in the experiment. Increasing the concentration does not result in the lengthening of the lobes, as it did, in the half-full square case. Instead, it changes the pattern altogether. For 30% by weight small particles, the pattern now has 5 "bumps" along its edges. These bumps correspond to the locations of period-5 islands in the Poincaré section generated by seeding seven initial points from the center of the tumbler to about half-way to the lower left corner (middle of the lower row of Fig. 4). As the concentration of small particles increases further to 50% by weight, the outer boundary of the pattern of small particles takes on a shape similar to the rings that lie to the outside of the period-5 islands in the corresponding Poincaré section (rightmost Poincaré section in the lower row of Fig. 4).

By using a polydisperse particle mixture (three different particle sizes), the symmetries of both the period-2 and period-5 islands can be captured simultaneously, as shown in Fig. 5. The mixture consists of 5% by weight 0.35 ± 0.02 mm particles (purple), 25% by weight 0.75 ± 0.02 mm particles (yellow), and 70% by weight 1.19 ± 0.04 mm particles (black). The smallest particles form two lobes resembling the period-2 islands in the Poincaré section of Fig. 3. The medium particles mimic the period-5 islands of the Poincaré section. The interface between the medium and large particles is blurred, because the ratio of particle diameter of large to medium particles is less than two, resulting in a relative weakening of segregation compared to collisional diffusion.

While the dynamics and segregation patterns can be altered by changing the shape of the tumbler, the pattern can also be changed by simply increasing the fill fraction of the square tumbler. In the half-full square, the maximum flowing layer length (and hence the streamwise velocity, v_x) occurs when the free surface intersects two opposing corners along the diagonal. For deviations from half-full, the free surface will intersect opposing corners along the diagonal at different points in rotation rather than simultaneously. Therefore, the flowing layer length has multiple maxima during each period of flow (one-quarter revolution for a square tumbler). Figure 6 shows a set of experiments and Poincaré sections for a 63%-full square tumbler, where the flowing layer length has two maxima during each period of the flow. In this case there is a small, unmixed core centered at the axis of rotation because these particles never reach the flowing layer (this core is not readily visible in Fig. 6). The Poincaré section has three period-3 islands near the unmixed core and five period-5 islands closer to the tumbler walls. Note that for the configuration shown, one of the period-3 regions is located within the flowing layer. Showing the tumbler in the diamond orientation (where the diagonal is horizontal) would reveal all three period-3 islands in the bed of solid body rotation. The segregation experiment with 10% by weight small particles shows three lobes (two of these lobes lie along the diagonals and one is in the flowing layer). At 30% by weight small particles, the boundary of the segregated small particles has five "bumps" corresponding to the period-5 islands in the Poincaré section. For 50% by weight small particles, the boundary of the segregated region displays the pattern outside of the period-5 islands of the Poincaré section. Thus, as with the half-full pentagonal tumbler, the segregation patterns in the 63%-full square tumbler appear to be governed by the dynamics of the underlying flow displayed in the Poincaré sections.

IV. RELATING PATTERNS AND DYNAMICS

Segregation patterns clearly mimic the dynamics of the underlying flow as revealed by the Poincaré sections. However, the connection is not expected because the computational model from which the Poincaré section is derived contains no information about particle properties or segregation. We study this phenomenon via techniques borrowed from analysis of fluid mixing [17,19], by comparing a 75%-full square tumbler to a half-full square tumbler. The 75%-full square tumbler proves to be an ideal case for demonstrating

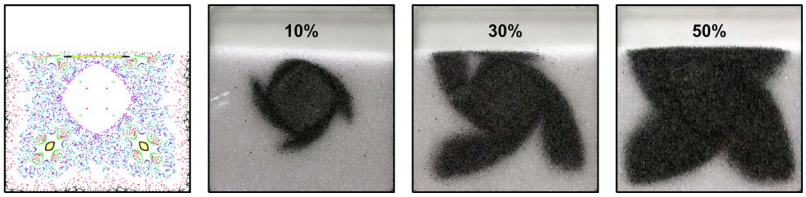

FIG. 7. (Color online) Poincaré section and segregation experiments with varying concentrations of small particles in a 75%-full square tumbler.

these techniques and gaining insight into the interplay of segregation and the underlying flow dynamics.

The Poincaré section of the 75%-full square has three period-3 elliptic points surrounded by islands (shown in Fig. 7) where, again, a period is defined as one-quarter revolution of the tumbler. Two of the islands are visible in the lower half of the Poincaré section. The third island is within the flowing layer near the free surface. Rotating the tumbler one-eighth revolution would show all three islands in the bed of solid body rotation. Surrounding the islands are regions of chaotic flow.

When the concentration of small particles is varied, the results are, at first glance, puzzling in comparison to those of the previous cases. In Fig. 7, all three experiments show patterns with some common features. There is an unmixed core of particles centered at the axis of rotation that do not enter the flowing layer at any point during rotation. At the low concentration of 10% by weight small particles, short "fingers" of small particles stretch toward the period-3 islands but do not reach them. This is similar to the low concentration experiments in the half-full square (Fig. 2) where the lobes point toward the islands without reaching them. As the concentration is increased to 30% by weight small particles, the lobes are thicker and reach out beyond the period-3 islands in the Poincaré section. Further increasing the concentration of small particles results in the lobes becoming thicker. However, for the 50% by weight small particles case, the lobes have grown thicker mostly on the clockwise side of the lobe as compared to the 30% case. In all cases, the lobes seems to curve or stretch clockwise from the core toward the period-3 islands. The lobes do not merely mark the islands for all small particle concentrations, but stretch toward them through the chaotic regions as the concentration is increased.

The underlying dynamics illustrated by the Poincaré section are a result of the time-periodic flow created here by tumbler geometry. By studying how the segregation patterns form in the experiment as a function of tumbler geometry and rotation, the connection between the symmetries of the Poincaré sections and segregation patterns can be better understood. The segregation patterns studied here tend to form very quickly, on the order of one to three tumbler revolutions. Figure 8 provides a series of images taken from frames of video footage during the early stages of an experiment, to follow the evolution to the steady segregation pattern in a 75%-full square tumbler with 30% by weight small particles. (The particle sizes in this case are slightly different than other experiments, as noted in the caption.) The initial condition is achieved by centrifuging and abruptly stopping the tumbler resulting in a homogeneous mixture (upper left image in Fig. 8). The initial condition appears black because the small black particles are mixed with the large clear particles. After one-half revolution (two periods), the particles that have passed through the layer have segregated to some extent. In a manner similar to the half-full square in Fig. 2, lobes of small particles stretch along paths where the flowing layer is increasing in length. After two periods as the tumbler in Fig. 8 rotates clockwise, the first stretch of the particles is toward corner B and the second stretch is toward corner A. After four periods of flow (one revolution), three lobes are visible. Note that the lobe that stretches toward corner A is partially within the flowing layer. The lobes are not static, but rotate with the elliptic points that characterize them in such a way that they point toward successive corners in a clockwise fashion after passing through the flowing layer. For example, the lobe that is pointing to C after four periods points to D after six periods as the lobe passes through the flowing layer. A stable pattern is formed in just six periods of flow (one and one-half revolutions).

Figure 9 shows the dynamics of the pattern over one-quarter revolution to illustrate the rotation of the lobes. The three lobes are all in the bed of solid body rotation when the tumbler is in the diamond configuration in Fig. 9(a). As the tumbler rotates clockwise, the left lobe at the tagged corner

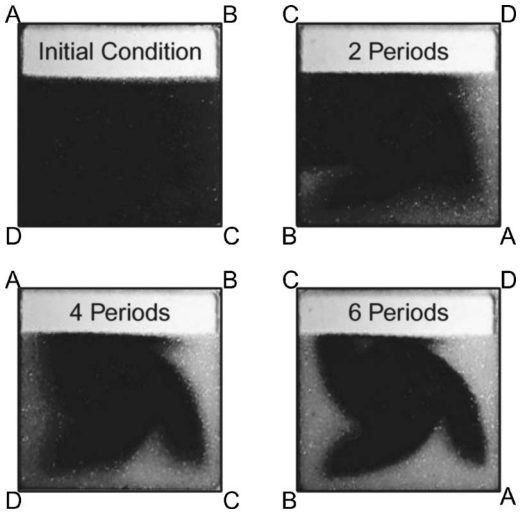

FIG. 8. Evolution of segregation pattern. Top left: initial condition. Top right: after $\frac{1}{2}$ revolution clockwise (2 periods). Bottom left: after 1 revolution (4 periods). Bottom right: after $1\frac{1}{2}$ revolutions (6 periods). 1.11 ± 0.10 mm clear glass beads and 0.35 ± 0.03 mm painted black glass beads. Letters label corners of the tumbler. Images captured by a video camera.

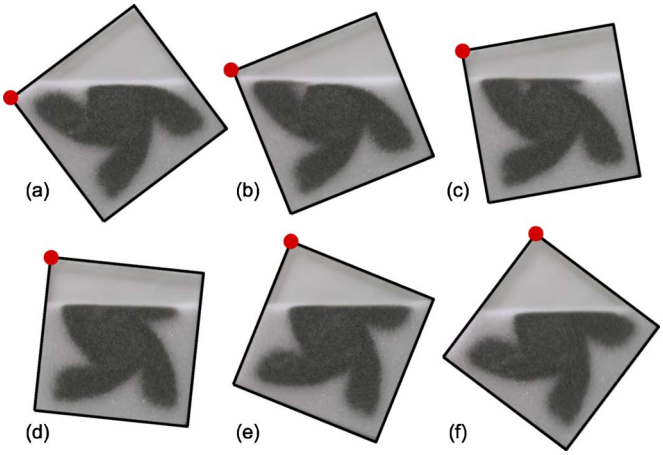

FIG. 9. (Color online) Orientation of the segregation pattern as the tumbler rotates clockwise through $\frac{1}{4}$ revolution for 30% by weight small particles in a 75%-full tumbler. A dot labels one corner of the tumbler. Images captured by a digital camera in continuous shooting mode.

in the image enters the flowing layer (b). As rotation continues, the small particles at the leading edge of the lobe drift toward the bottom of the layer connecting with the core (c). The length of the flowing layer increases as it approaches a corner on the right side (d). Small particles behind the leading edge therefore remain in the flowing layer longer and flow over the first small particles, stretching toward the corner (e). The particles that formed the base of the original lobe form the tip of the new lobe (f). The net effect of this process is a clockwise rotation of the particles within the lobe so that after one period the lobe points to the corner that is ahead of the original tagged corner.

The observations from the evolution toward the steady pattern in Fig. 8 and of the motion of the segregation pattern with respect to the tumbler in Fig. 9 provide insight into how the segregation experiments mimic the underlying flow that defines the Poincaré sections. The particles in the segregation experiment do not simply fill in the regions occupied by the islands in the Poincaré sections. Instead, the segregation pattern is also governed by the chaotic regions of flow related to the hyperbolic points in the Poincaré sections. Thus, the segregation patterns in Figs. 2 and 7 are a result of the driving forces of segregation and the effect of time-periodic flow in the chaotic regions due to tumbler geometry orientation.

V. INSIGHTS FROM EIGENVALUE/EIGENVECTOR ANALYSIS

A distinguishing characteristic between the segregation experiments of the half-full and 75%-full square tumblers is the direction in which the lobes curve. The images of the half-full square tumbler in Fig. 2, particularly at lower concentrations, show lobes curving or stretching in a counterclockwise direction. Conversely, the lobes in the 75%-full square shown in Fig. 7 curve and stretch in a clockwise direction. To gain some insight into this aspect of the segregation pattern, we turn to analysis of the eigenvalues and

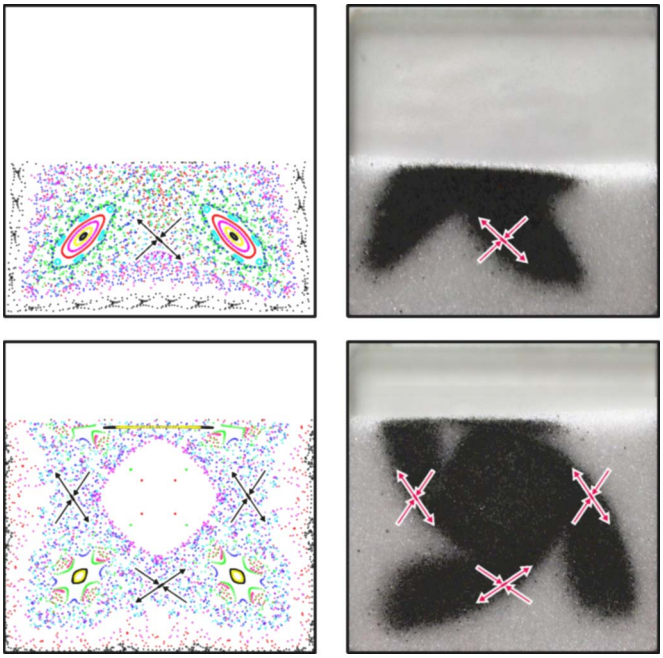

FIG. 10. (Color online) The eigenvectors for hyperbolic points in a half-full square tumbler (top) and 75%-full square tumbler (bottom) with the arrowheads showing the direction of stretching and compression as determined from the eigenvalues. The experimental pictures are mixtures of 20% small particles for the half-full square and 30% small particles for the 75%-full square.

eigenvectors of the hyperbolic points, a technique borrowed from the study of chaotic fluid flows. For both the half-full and 75%-full tumblers the hyperbolic points are located along the lines from the center of the tumbler to the midpoint of the sides, between the islands evident in the Poincaré sections. Figure 10 shows the direction of the eigenvectors for the hyperbolic points superimposed over both the Poincaré sections and experimental images for the two cases. For the half-full square, in the orientation shown, one of the two hyperbolic points is within the flowing layer (not shown). In both cases, the eigenvectors corresponding to stretching are directed along one side of a lobe. The lobes for these two cases stretch from the hyperbolic points in the direction given by the stretching eigenvector and curve toward a corner of the tumbler. Physically, the stretch corresponds to the lengthening of the flowing layer which occurs in these systems when the free surface approaches a corner. Thus, the opposite curvature of the lobes for the two cases in Fig. 10 arises from the stretching eigenvectors pointing in the direction of opposite corners.

The rotation of the lobes with respect to the tumbler, shown in Fig. 9, can be further explained in terms of stretching at hyperbolic points. Figure 11 shows the location of a single hyperbolic point and its eigenvectors for a series of rotational positions of the 75%-full tumbler. The outline of the tumbler configurations at the approximate times in which the hyperbolic point enters and exits the flowing are shown with dotted lines. Until the hyperbolic point reaches the flowing layer, the eigenvectors move around the center of the tumbler in solid body rotation. When the hyperbolic point reaches the flowing layer, the stretching eigenvector rotates

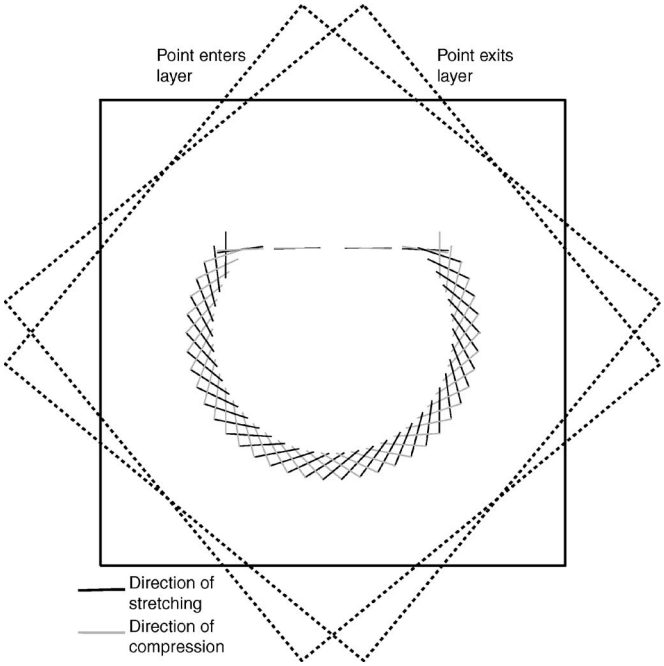

FIG. 11. Eigenvectors of a period-3 hyperbolic point for varying rotational position of the tumbler. The dotted lines show the configuration of the tumbler when the hyperbolic point enters and exits the flowing layer.

such that its direction is nearly the same as that of the compression eigenvector. This is due to the high shear within the flowing layer. The deformation in the flowing layer is mainly stretching in the streamwise direction. When the hyperbolic point exits the flowing layer and re-enters the bed of solid body rotation, the compression eigenvector rotates such that the angle between the two eigenvectors is identical to the angle before the hyperbolic point entered the flowing layer. Thus, the stretching eigenvector initially pointed toward the upper corner (as it enters the layer) stretches toward the right corner (as it flows in and leaves the layer) rotating the eigenvector with respect to the tumbler. This is directly related to the rotation of the segregation pattern shown in Fig. 9. The eigenvectors in Fig. 11 rotate in the same manner as the lobes in the segregation pattern in Fig. 9.

VI. FURTHER INSIGHT FROM MANIFOLD ANALYSIS

An extension of the eigenvector analysis is to consider manifolds associated with the hyperbolic points. A *stable* manifold for a hyperbolic point **P** is the set of points in the tumbler that approach **P** as the number of mappings applied approaches infinity. Similarly, an *unstable* manifold is the set of points that approaches **P** as inverse mappings are applied (equivalent to running time in reverse). The stretching eigenvector is tangent to the unstable manifold at **P** and the compression eigenvector is tangent to the stable manifold at **P**. A circle of points seeded around a hyperbolic point will move in the directions of stretching, tracing the unstable manifold. From here, the points follow a path that leads them toward another hyperbolic point (or back to the original) approaching from the direction of the compression eigenvector. However, in chaotic systems the unstable manifold will often not join the stable manifold but rather cross it many times during the approach to a hyperbolic point [19]. Figure 12 shows a manifold analysis for a 75%-full square using the method of Swanson *et al.* in which a very small ring of points is placed around a hyperbolic point and allowed to advect for a certain number of periods [17]. The points are plotted every time the hyperbolic point returns to its original location (for this case, every cycle of three periods of flow, since the hyperbolic points are period-3). In the time evolution plots shown in Fig. 12, the curves stretch toward hyperbolic points and then fold over themselves. The curves eventually stretch toward other hyperbolic points, again folding over themselves as they approach the hyperbolic point. Three unstable manifolds (one beginning at each hyperbolic point) are superimposed over an experimental image with 30% small particles by weight. The trajectories follow along the edges of the lobes. The folding near hyperbolic points on the outside of the segregated pattern corresponds with areas that contain only large particles for this particular fraction of small particles, effectively mapping the boundary between small and large particles. In some sense, the manifold analysis is an integrated view of the effect of the chaotic regions on the flow. Whereas the stretching eigenvectors reveal the rotational orientation of the segregation pattern (clockwise or counterclockwise), the unstable manifolds reveal how the pattern changes (how the lobes will curve) as the small particle concentration is increased. This further demonstrates that the segregation that occurs in the flowing layer is connected with areas in which stretching is occurring, resulting in the final segregation pattern.

VII. CONCLUSIONS

We have made arguments about the connection between the underlying granular flow as evidenced by the Poincaré

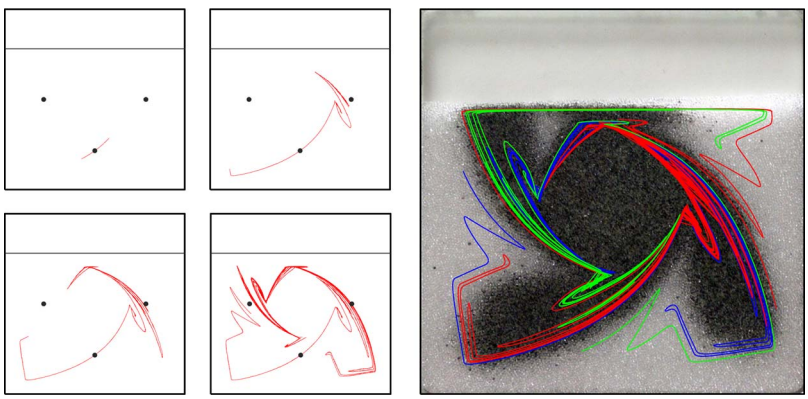

FIG. 12. (Color online) Unstable manifold analysis for a 75%-full square tumbler. The locations of the hyperbolic points are shown with dots. Left: plots after 4, 6, 8, and 10 three-period cycles. Right: unstable manifolds after 10 three-period cycles overlaid on an experimental picture of a mixture with 30% small particles.

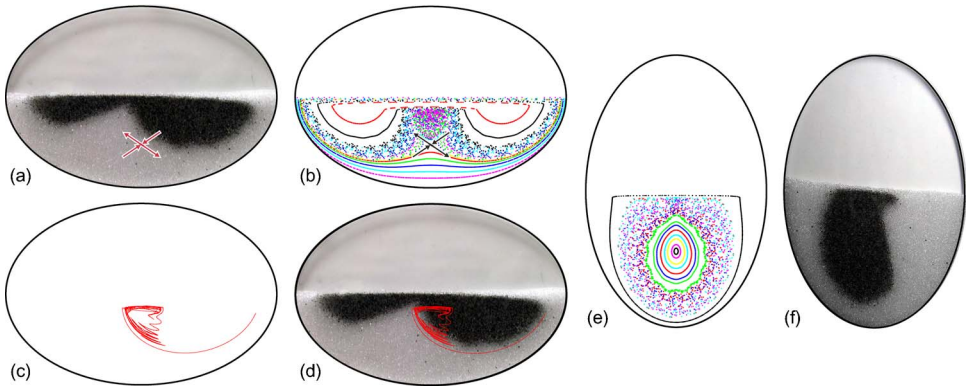

FIG. 13. (Color online) Elliptical tumbler. (a) Segregation experiment (21.5 cm major axis, 14.4 cm minor axis) with 20% by weight small particles with hyperbolic point and corresponding eigenvectors labeled. (b) Poincaré section with major axis horizontal. (c) Manifold tracing. (d) Overlay of segregation experiment with manifold tracing. (e) Poincaré section with minor axis horizontal showing a single island. (f) Segregation experiment with minor axis horizontal showing a single lobe.

sections and segregation patterns using examples of half-full and greater than half-full polygonal tumblers. Time periodicity arises from rotational orientation of the tumbler geometry, so that the flowing layer thickness, shape, and velocity field, Eqs. (2)–(4), become functions of time [18]. In the segregation experiments shown here, particles are sorted in the flowing layer; large particles rise to the top and small particles percolate to the bottom. Once segregated, the particles flow as if they were monodisperse. The large particles are subject to the dynamics of the flow in the top portion of the flowing layer which corresponds to the outermost regions of the Poincaré section. The small particles are subject to the dynamics in the bottom portion of the flowing layer which corresponds to the innermost regions of the Poincaré section. In Figs. 4 and 6 the segregation patterns resemble the islands in the Poincaré sections. However, the patterns do not merely mark the islands, but are also influenced by the chaotic regions. In the cases of the half-full and 75%-full square, lower particle concentrations do not even reach the islands shown by Poincaré sections (Figs. 2 and 7). Here the small particles are only subject to the dynamics of the chaotic regions. Figures 9–11 show that the orientation of the lobes in the segregation patterns correspond to the orientation of the eigenvectors of the hyperbolic points that characterize the chaotic regions. Thus, coupling the knowledge of the symmetries of the Poincaré sections with a knowledge of the dynamics in the chaotic regions, reveals the general features of the segregation pattern (rotational orientation and shape of the lobes), and how these patterns vary as a function of small particle concentration. It is remarkable that a simple model taking into account only gross aspects of segregation is capable of capturing patterns in such a faithful way. The reason for this agreement is that the dynamics is dominated by geometrical aspects rather than details of the dynamics taking place at the particle level.

This analysis can in fact be applied generally to many different time-periodic granular flows. For example, in addition to studying even and odd sided polygonal tumblers of varying fill fractions, smooth geometries such as an elliptical tumbler can be considered. The ellipse is interesting because unlike a polygon, the flowing layer length and depth vary smoothly (dL/dt is a continuous function). In a half-full elliptical tumbler, the flowing layer length and the streamwise velocity are at a maximum when the free surface is along the major axis and at a minimum when the free surface is along the minor axis. Over one revolution of the tumbler, the maximum is reached two times. Therefore the period for this system is one-half revolution. There is only one island in the Poincaré section for a half-full elliptical tumbler shown in Fig. 13(b). With the major axis along the horizontal, this island is stretched through the flowing layer with equal amounts on both the left and right in the fixed bed. Rotating the tumbler one-quarter revolution shows the island completely in the bed of solid body rotation [Fig. 13(e)].

For a mixture of 20% by weight small particles, shown in Fig. 13(a), there are more small particles on the right side than the left. This asymmetry is reminiscent of the asymmetry observed in the half-full square in Fig. 2. Upon first glance there appears to be two lobes in the segregation experiment, however, when shown with the free surface along the minor axis [Fig. 13(f)], there is only one lobe which corresponds to the single island shown in the Poincaré section [Fig. 13(e)]. By considering the direction of stretching at the hyperbolic point, it is clear that the unstable manifold traces the location of the right half of the pattern, similar to the observations for the 75%-full square tumbler in Fig. 12.

The analysis presented here can be further applied to granular flows in quasi-2D tumblers that are time periodic not through the geometry, but due to a time-periodic rotation rate [32]. Figure 14 illustrates how the analysis applies to the case of a circular tumbler with a time-periodic rotation rate of the following form:

$$\omega = \omega_{\text{ave}} + \omega_{\text{amp}} \sin(2\pi f_e t), \tag{7}$$

where ω_{ave} is the average rotation rate and where $\omega_{\text{ave}} \pm \omega_{\text{amp}}$ is in a range where the flow is in the continuous-flow regime. The forcing frequency is given by f_e. In the case of Fig. 14, $f_e = 4$. This means that the rotation rate reaches a maximum four times and a minimum four times during one revolution of the tumbler. Thus the period of flow is one-quarter revolution (analogous to the square tumbler). The flowing layer

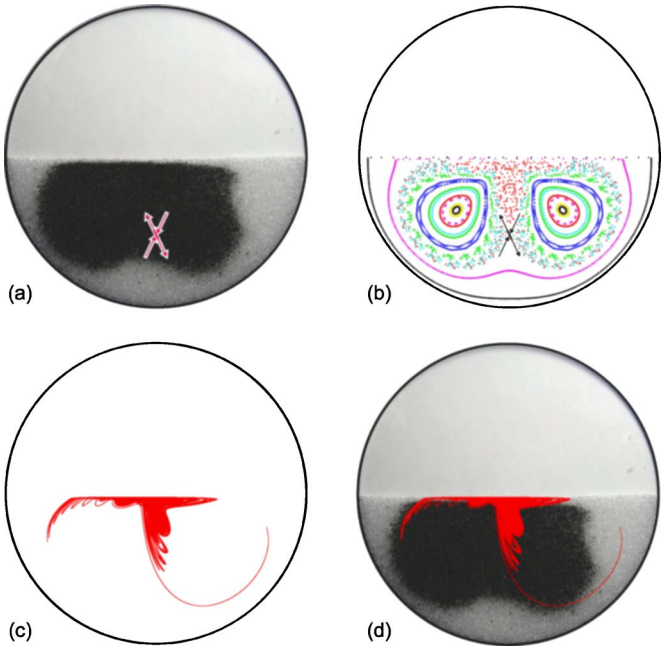

FIG. 14. (Color online) Time periodic forcing of a circular tumbler. (a) Segregation experiment in a circular tumbler, 20 cm diameter, with the hyperbolic point and corresponding eigenvectors labeled. (b) Poincaré section with the hyperbolic point and corresponding eigenvectors. (c) Manifold tracing. (d) Overlay of segregation experiment with manifold tracing.

thickness varies with the rotation rate [32–34]. When the rotation rate increases, so does the flowing layer thickness. In both the rotating half-full square and the time-periodically rotated half-full circle with $f_e=4$ there are two period-2 islands in the Poincaré section and two lobes of small particles in the segregation experiment. The segregation pattern in Fig. 14 shows the same clockwise rotation from the Poincaré section evident in the half-full square. There are also similarities between the time-periodic circular tumbler and the half-full square tumbler in terms of the direction of the stretching eigenvector (compare to Fig. 10).

The techniques presented here can be applied very broadly to any quasi-2D tumbler geometry. Furthermore, the interplay between segregation and the underlying flow dynamics may be applicable to granular flows in three-dimensional (3D) tumblers. We can construct the flow skeleton made up of the arrangement and interaction of the periodic points and periodic lines in a 3D time-periodic granular flow. Key questions are if the analogy between the segregation experiments and symmetries of the underlying flow dynamics still hold in 3D tumblers and how these analogies can be utilized and visualized in the substantially more complex 3D systems. Extending this approach to more complex flow systems will certainly demand further advances in the tools and techniques for analyzing chaotic systems.

ACKNOWLEDGMENTS

We wish to acknowledge Stan Fiedor for experimental assistance and Paul Umbanhowar for insightful conversations. This work was funded in part by the Office of Basic Energy Sciences of the Department of Energy (Grant No. DE-FG02-95ER14534). S.W. Meier acknowledges support from the National Science Foundation.

[1] K. M. Hill, D. V. Khakhar, J. F. Gilchrist, J. J. McCarthy, and J. M. Ottino, Proc. Natl. Acad. Sci. U.S.A. **96**, 11701 (1999).
[2] J. Duran, *Sands, Powders, and Grains: An Introduction to the Physics of Granular Materials* (Springer, New York, 2000).
[3] G. H. Ristow, *Pattern Formation in Granular Materials*, Springer Tracts in Modern Physics, Vol. 164 (Springer, Berlin, 2000).
[4] J. M. Ottino and D. V. Khakhar, Annu. Rev. Fluid Mech. **32**, 55 (2000).
[5] G. H. Ristow, Europhys. Lett. **28**, 97 (1994).
[6] N. Jain, J. M. Ottino, and R. M. Lueptow, Granular Matter **7**, 69 (2005).
[7] N. Jain, J. M. Ottino, and R. M. Lueptow, Phys. Rev. E **71**, 051301 (2005).
[8] J. Bridgwater, N. W. Sharpe, and D. C. Stocker, Trans. Inst. Chem. Eng. **47**, T114 (1969).
[9] F. Cantelaube and D. Bideau, Europhys. Lett. **30**, 133 (1995).
[10] E. Clément, J. Rajchenbach, and J. Duran, Europhys. Lett. **30**, 7 (1995).
[11] C. M. Dury and G. H. Ristow, J. Phys. I **7**, 737 (1997).
[12] H. Henein, J. K. Brimacombe, and A. P. Watkinson, Metall. Trans. B **14**, 191 (1983).
[13] M. Nakagawa, S. A. Altobelli, A. Caprihan, E. Fukushima, and E. K. Jeong, Exp. Fluids **16**, 54 (1993).
[14] J. Rajchenbach, Phys. Rev. Lett. **65**, 2221 (1990).
[15] D. V. Khakhar, J. J. McCarthy, and J. M. Ottino, Phys. Fluids **9**, 3600 (1997).
[16] T. Elperin and A. Vikhansky, Chaos **9**, 910 (1999).
[17] P. D. Swanson and J. M. Ottino, J. Fluid Mech. **213**, 227 (1990).
[18] D. V. Khakhar, J. J. McCarthy, J. F. Gilchrist, and J. M. Ottino, Chaos **9**, 195 (1999).
[19] J. M. Ottino, *The Kinematics of Mixing: Stretching, Chaos, and Transport* (Cambridge University Press, Cambridge, 1989).
[20] A. Kolmogorov, Dokl. Akad. Nauk SSSR **98**, 527 (1954).
[21] A. Kolmogorov, in *1954 Congress in Mathematics* (North-Holland, Amsterdam, 1954), pp. 315–333; translated as Appendix in R. H. Abraham and J. E. Marsden, *Foundations of Mechanics* (Benjamin/Cummings, Reading, 1978) pp. 741–757.
[22] V. Arnold, Russ. Math. Surveys **18**, 85 (1963).
[23] J. G. Franjione and J. M. Ottino, Philos. Trans. R. Soc. London, Ser. A **338**, 301 (1992).
[24] R. C. Hilborn, *Chaos and Nonlinear Dynamics: An Introduction for Scientists and Engineers*, 2nd edition (Oxford Univer-

sity Press, Oxford, 2000).
[25] A. J. Lichtenberg and M. A. Lieberman, *Regular and Chaotic Dynamics* 2nd edition, Applied Mathematical Sciences, Vol. 38 (Springer-Verlag, New York, 1992).
[26] J. M. Ottino, Phys. Fluids A **3**, 1417 (1991).
[27] S. E. Cisar, P. B. Umbanhowar, and J. M. Ottino (unpublished).
[28] N. Jain, J. M. Ottino, and R. M. Lueptow, Phys. Fluids **14**, 572 (2002).
[29] T. S. Krasnopolskaya, V. V. Meleshko, G. W. M. Peters, and H. E. H. Meijer, Eur. J. Mech. B/Fluids **18**, 793 (1999).
[30] K. M. Hill, G. Gioia, and D. Amaravadi, Phys. Rev. Lett. **93**, 224301 (2004).
[31] K. M. Hill, G. Gioia, D. Amaravadi, and C. Winter, Complexity **10**, 79 (2005).
[32] S. J. Fiedor and J. M. Ottino, J. Fluid Mech. **533**, 223 (2005).
[33] D. V. Khakhar, A. V. Orpe, and J. M. Ottino, Adv. Complex Syst. **4**, 407 (2001).
[34] H. A. Makse, Phys. Rev. Lett. **83**, 3186 (1999).